J Mol Model (2010) 16:107–118
DOI 10.1007/s00894-009-0523-0

ORIGINAL PAPER

Hemolytic mechanism of dioscin proposed by molecular dynamics simulations

Fu Lin · Renxiao Wang

Received: 18 February 2009 / Accepted: 9 April 2009 / Published online: 10 June 2009

Abstract Saponins are a class of compounds containing a triterpenoid or steroid core with some attached carbohydrate modules. Many saponins cause hemolysis. However, the hemolytic mechanism of saponins at the molecular level is not yet fully understood. In an attempt to explore this issue, we have studied dioscin—a saponin with high hemolytic activity—through extensive molecular dynamics (MD) simulations. Firstly, all-atom MD simulations of 8 ns duration were conducted to study the stability of the dioscin–cholesterol complex and the cholesterol–cholesterol complex in water and in decane, respectively. MM-GB/SA computations indicate that the dioscin–cholesterol complex is energetically more favorable than the cholesterol–cholesterol complex in a non-polar environment. Next, several coarse-grained MD simulations of 400 ns duration were conducted to directly observe the distribution of multiple dioscin molecules on a DPPC-POPC-PSM-CHOL lipid bilayer. Our results indicate that dioscin can penetrate into the lipid bilayer, accumulate in the lipid raft micro-domain, and then bind cholesterol. This leads to the destabilization of lipid raft and consequent membrane curvature, which may eventually result in the hemolysis of red cells. This possible mechanism of hemolysis can well explain some experimental observations on hemolysis.

Keywords Hemolysis · Saponin · Molecular dynamics · Coarse-grained model

Electronic supplementary material The online version of this article (doi:10.1007/s00894-009-0523-0) contains supplementary material, which is available to authorized users.

F. Lin · R. Wang (✉)
State Key Laboratory of Bioorganic Chemistry, Shanghai Institute of Organic Chemistry, Chinese Academy of Sciences,
345 Lingling Road,
Shanghai 200032, People's Republic of China
e-mail: wangrx@mail.sioc.ac.cn

Introduction

Saponins are named after their ability to form soap-like foams in aqueous solution. In chemical terms, a saponin molecule contains a carbohydrate segment attached to a triterpenoid or steroid moiety. Most saponins are highly surface-active, and many exhibit a general tendency to cause hemolysis and other biological and pharmacological effects, such as antitumor and cardioactive effects. Furthermore, saponins have plasma cholesterol-lowering activity. They are widely utilized as a component of ISCOMATRIX (immunostimulation complex) adjuvant, which is safe and induces both humoral and cellular immune responses when complexed with cholesterol [1]. Saponins are attracting considerable interest as a result of their diverse properties, both deleterious and beneficial [2].

One of the most important features of saponins is their hemolytic activity. It has long been studied and the origin of this phenomenon is generally ascribed to the amphiphilic properties of saponins [3]. However, the exact mechanism remains as yet unknown, especially in the light of the structural diversity of saponins. For a series of model compounds (such as digitonin) it was demonstrated that neither the surface nor the interfacial tension-lowering properties of saponins can be correlated with their ability to induce hemolysis [4]. It was observed that the hemolytic activity of saponins is proportional to the number of saccharide units in their chemical structures, and those derivatives with branched saccharide chains exhibited higher activities than those with straight chains [5]. However, the structure–activity relationship of these compounds has not been studied at the molecular level, and what factors affect their hemolytic activity remain to be explored.

So far, the hemolytic activity of saponins is generally believed to be the result of the affinity of the aglycone

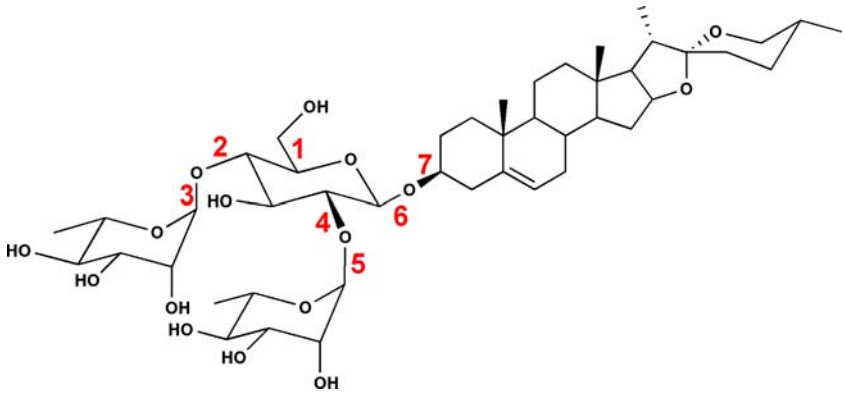

Fig. 1 Chemical structure of dioscin. *Numbers* denote the seven rotatable single bonds considered in conformational sampling

moiety to membrane sterols, in particular cholesterol [2, 6], with which they form insoluble complexes. It is well known that saponins, such as digitonin, bind strongly to cholesterol to form rigid equimolecular complexes, and other saponins are also believed to interact with cholesterol. In the case of erythrocytes, complex formation results in rapid cell lysis [7] and leads to membrane disintegration in the presence of relatively high digitonin concentrations. Digitonin forms such strong and stable complexes with cholesterol that it is used for cholesterol measurement in blood plasma, bile, and tissues [8]. Furthermore, Toshiyuki Akiyama et al. [9] demonstrate through ^{2}H-NMR spectra that cholesterol complexed with digitonin (equimolar complex) exists as solid-state-like digitonides in a lipid bilayer. Unfortunately, the complex structure is still unknown.

In this study, we have attempted to understand the hemolytic process of saponins from the perspective of conformation analysis and molecular dynamics (MD) simulations. We chose dioscin as a representative saponin for our purposes. Dioscin (Fig. 1) exhibits potent hemolytic activity (hemolytic dose for 50% hemolysis, $HD_{50} = 3.0 – 3.4$ μM) [5, 10]. To gain some insights into the interaction of dioscin with cholesterol, and to discuss the mechanism of its hemolytic effect, all-atom MD simulations were conducted to explore the possible binding modes between dioscin and cholesterol in water, decane, and a decane/water two-phase system, and coarse-grained molecular dynamics (CGMD) simulations were conducted to observe the penetration of dioscin into a lipid membrane, and the aggregation of dioscin into lipid rafts. A possible hemolytic mechanism of dioscin is proposed according to our simulation results.

Methods

Conformational sampling of dioscin in vacuum

The three-dimensional structure of dioscin was constructed through molecular modeling since it has not yet been resolved by experimental means. The structure of the steroid moiety on dioscin was taken directly from its counterpart on the crystal structure of cholesterol isobutyl carbonate [11]. The rest of the dioscin molecule was sketched using SYBYL software [12]. The structural model was then optimized until the energy gradient was lower than 0.01 kcal mol^{-1} Å^{-1}. The Tripos force field and the Gasteiger-Hückel partial charges were used in this process.

A systematic conformational search with respect to the seven rotatable single bonds on dioscin (see Fig. 1) was conducted. Each rotatable single bond was sampled with an increment of 15°. Apparently, this process would produce a huge number of conformations—up to $(360/15)^7 = 4.6 \times 10^9$ possible conformations. A cutoff of 10 kcal mol^{-1} was therefore applied to select low-energy conformations from among all outcomes for subsequent analysis. Application of this filter resulted in a total of 2,516 conformations. These were subjected to structural optimization using the same setting as specified above. These minimized conformations were then clustered using the MATLAB program to select representative conformations. A detailed description of this process is given in the electronic supplementary material (ESM).

It should be noted that we actually tested three different fitting algorithms as well as three fitting methods in our cluster analysis. We also tested the root mean squares (RMS)-analysis toolkit in the GOLD program (version 3.2) [13] for this purpose (Table S1). All of these efforts produced basically the same outcomes, indicating that our results were independent from the computational tools. Based on these results (Table S2), we concluded that dioscin had two major families of low-energy conformations in vacuum, in which CNF_32181 was the more populated. Accordingly, we adopted CNF_32181 as the typical conformation in vacuum for subsequent simulations.

MD simulations of dioscin in water and in decane

MD simulations were adopted to sample possible conformations of CNF_32181 in water and in decane. Simulations were conducted using the AMBER (version 7.0) [14] and

GROMACS (version 3.3) [15] programs, respectively. To set up the MD simulation, the electrostatic potentials of dioscin was computed using the Gaussian 98 software [16] at the HF/6-31G* level. Atom-centered partial charges were derived using the restrained electrostatic potential (RESP) method [17]. Dioscin was soaked in a TIP3P [18] water box (50 Å × 38 Å × 32 Å) and a decane box (105 Å × 105 Å × 105 Å), respectively. Periodic boundary conditions were applied to all dimensions. The particle mesh Ewald (PME) method [19] was applied to calculate long-range electrostatic interactions, in which the interpolation order was set to four. The time interval in simulation was set to 1 fs.

For MD simulations of dioscin in water done by AMBER, the entire system was minimized in two consecutive rounds, each of which consisted of 3,000 steps. Harmonic constraints were applied to all non-hydrogen atoms on dioscin with a strength of 500 and 0 kcal mol^{-1} $Å^{-2}$ at each round. The system was then heated from 0 to 300 K in 7.5 ps and equilibrated at 300 K for another 12.5 ps. A subsequent production run was performed at a constant temperature of 300 K and a constant pressure of 1 atm, giving a total simulation time of 5 ns. The general AMBER force field (GAFF) [20] was adopted in simulations since it was developed to handle small organic molecules. No constraint was applied to dioscin during MD simulation. For MD simulation of dioscin in decane done by GROMACS, the entire system was minimized to convergence using the steepest descent method. The compound was in position restraint MD simulation at 300 K for 500 ps. A subsequent production run was performed at a constant temperature of 300 K and a constant pressure of 1 atm, giving a total simulation time of 5 ns.

Analysis of each resulting MD trajectory focused on its equilibrium stage. RMSD of dioscin (Fig. S1) was calculated from the trajectory by using the initial conformation as the reference. Snapshots were taken from MD trajectory with an interval of 1 ps. The MM-GB/SA method [21], which is implemented in AMBER, was applied to compute free energies. Cluster analysis of the MD trajectory was performed by the MMTSB tool set [22]. The technical details of the MM-GB/SA computations and cluster analysis are given in the ESM.

Cluster analysis indicated that dioscin had two clusters of low-energy conformations in water (Table S3). The ratio between these two clusters was almost 1:1, and the oligosaccharide moiety of dioscin was basically perpendicular to the steroid moiety in both clusters. These two types of conformations were somewhat different from those obtained in vacuum (Table S2). The predominant low-energy conformations of dioscin in decane (Table S4) were similar to those in water. The representative low-energy conformations of dioscin in water (REC04235) and in decane (REC02570) were used in the subsequent MD simulations.

MD simulations of the dioscin–cholesterol complex and the cholesterol–cholesterol complex

To understand the mechanism of hemolytic activity, we studied the binding of dioscin with cholesterol. The coordinates of cholesterol were extracted from the available crystal structure of cholesterol derivatives [23–25]. Cholesterol was docked manually to dioscin using the COMPUTE module in the SYBYL software (version 7.2) with the MMFF94 force field (Table S5 and Fig. 2). Dioscin adopted the most populated conformation derived from the MD sampling of dioscin in water and in decane at the previous step.

After docking, MD simulation of the dioscin–cholesterol complex and the cholesterol–cholesterol complex in water and in decane were conducted by AMBER and GROMACS, respectively. All parameters for these MD simulations were similar to those used in the previous step. The MD simulations lasted for 8 ns with a sampling interval of 2 ps. The following cluster analysis was based on the 3,500 snapshots sampled from the last 7 ns on the resulting MD trajectories, and we obtained the binding mode of dioscin-cholesterol complex in water and in decane. Cluster analysis was done with the MMTSB tool set. Then, combined with MM-GB/SA binding free energy, we picked out the conformation with the lowest binding free energy within each cluster as the representative standing for each cluster (Table 1, Fig. 3, Fig. S2 and Fig. S3).

Another two simulations were performed in the decane/water two-phase system. Both models were soaked in a periodic, two-phase cubic box. Model 1 (see Fig. 4a) contained 962 decane molecules and 16,017 water molecules. Dioscin was placed in water, while cholesterol was placed in decane. The distance between dioscin and cholesterol was about 13 Å. Model 2 (see Fig. 4b) contained 1,131 decane molecules and 12,892 water molecules. Dioscin and cholesterol were both immersed in decane in such a way that the oligosaccharide moiety of dioscin pointed toward the decane phase. The initial binding mode is shown in Fig. 4b. MD simulations of this system were then performed using GROMACS. The parameter setup for this simulation was similar to the simulation in decane. The system was initially minimized for 8,000 steps with the steepest descent method, and then a 500 ps position-restrained MD simulation was conducted with a force constant of 100 kJ mol^{-1} $Å^{-1}$. For both models, an 11 ns production run was carried out at 300 K and 1 atm.

CGMD simulations of the behavior of dioscin on the lipid bilayer

The MARTINI force field [26] of DPPC (1,2-dipalmitoyl-sn-glycero-3-phosphocholine) was adopted in our CGMD simulations. The steroid moiety on dioscin is very similar

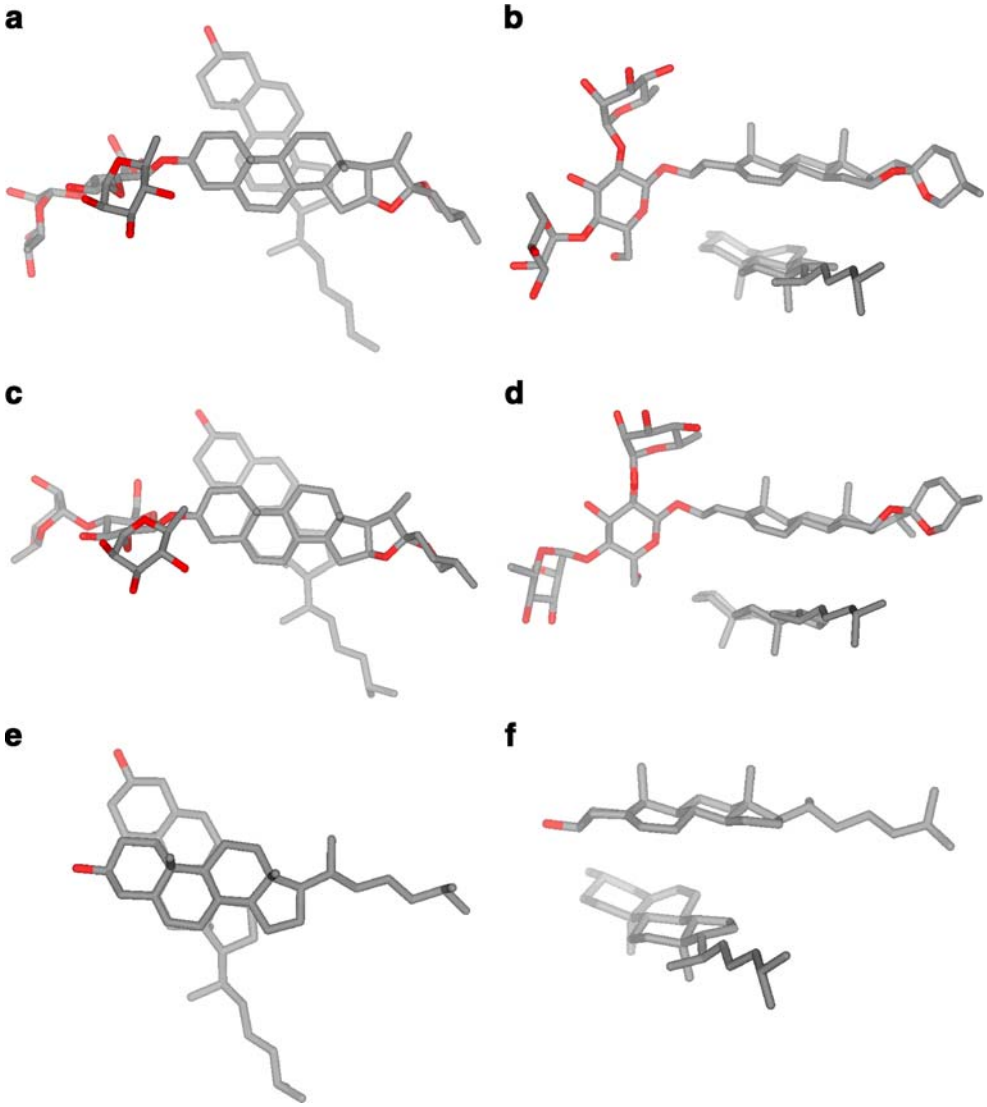

Fig. 2 Docking results of the dioscin–cholesterol and cholesterol–cholesterol complexes (*left* top view, *right* side view)

to cholesterol, whose CG interaction sites have already been given in the MARTINI force field II. The required parameters for the other parts of dioscin were deduced using Marrink's method [26] in our study. The coarse-grained scheme of dioscin is shown in Fig. S4. Dioscin was initially placed on the top of the well equilibrated DPPC bilayer (Fig. 5a).

We used a DPPC-POPC-PSM-CHOL lipid bilayer model in our simulation, which was composed of 1,644 DPPC molecules, 256 POPC (1-palmitoyl-2-oleoyl-sn-glycero-3-

Table 1 Conformational clusters of the dioscin–cholesterol complex sampled by molecular dynamics (MD) simulations in decane and in water. *RMSD* Root mean square deviation

	Cluster	Number of conformations	Percentage	ΔG (kcal/mol)[a]	RMSD (Å)[b]
In decane	D-1	2,535	72.43%	-26.87	3.6769
	D-2	965	27.57%	-40.51	5.7387
In water	W-1	395	11.29%	-25.40	2.0506
	W-2	99	2.83%	-22.64	3.6574
	W-3	595	17.00%	-22.79	3.6396
	W-4	557	15.91%	-24.92	2.7312
	W-5	451	12.89%	-27.06	3.8953
	W-6	993	28.37%	-26.90	2.1634
	W-7	410	11.71%	-23.43	4.3740

[a] Binding free energy of the typical conformation in each cluster computed by MM-GB/SA

[b] Calculated using the initial structure as reference

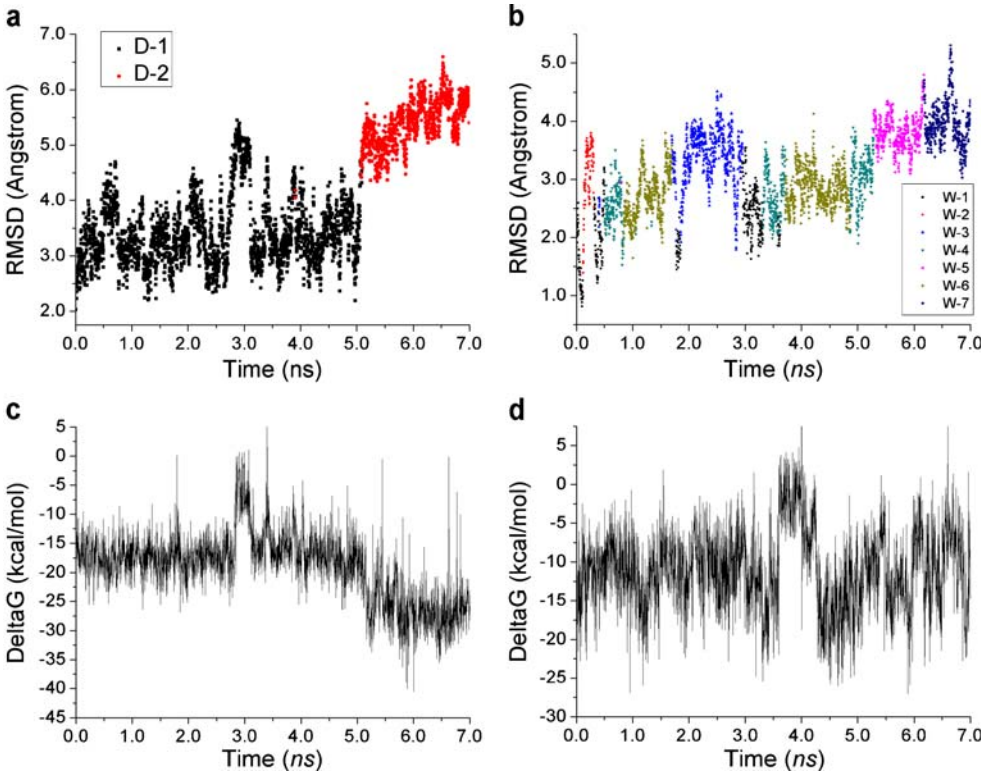

Fig. 3 **a** Root mean square deviation (RMSD) of the dioscin–cholesterol complex during the last 7 ns of molecular dynamics (MD) simulation in decane. **b** RMSD of the dioscin-cholesterol complex during the last 7 ns of MD simulation in water. Different colors denote different clusters of conformations. RMSD was calculated using the initial conformation as reference. **c** Binding free energy of the dioscin-cholesterol complex during MD simulation in decane. **d** Binding free energy of the dioscin-cholesterol complex during MD simulation in water

phosphocholine) molecules, 128 PSM (N-palmitoyl-D-erythro-sphingosylphosphorylcholine) molecules, and 128 CHOL (cholesterol) molecules. Usually, POPC-PSM-CHOL (in which POPC: PSM: CHOL = 256: 128: 128) is used to model the lipid raft micro-domain [27]. However, the MARTINI force field II for POPC-PSM-CHOL cannot well reproduce the average area per lipid of POPC-PSM-CHOL, which is given by all-atom simulations [27]. Thus, we had to re-parameterize the force field for POPC-PSM-CHOL. Because the net charge of CG interaction sites on the carbon chain of the lipid was zero, we could adjust only some Lennard-Jones parameters of the interaction sites in MARTINI force field II to reproduce the average area per lipid molecule on the POPC-PSM-CHOL bilayer through trial-and-error. The optimal Lennard-Jones parameters for PSM are given in Table S6.

The fully hydrated DPPC-POPC-PSM-CHOL bilayer model was first subjected to a CGMD simulation of 400 ns duration to ensure that it was well equilibrated (see Figs. S5, S6). We then added three dioscin molecules on top of the DPPC-POPC-PSM-CHOL membrane in the water phase and then subjected this system to a CGMD simulation (Fig. 6). To observe the effect of large number of dioscins on the lipid raft micro-domain (POPC-PSM-CHOL), four additional CGMD simulations of POPC-PSM-CHOL-DIOSCIN with different compositions (POPC:PSM:CHOL:dioscin = 256:128:128:0, 256:128:128:32, 256:128:128:64, and 256:128:128:128) were performed. In the initial configurations of these simulations, dioscin molecules were distributed evenly in one leaflet of the POPC-PSM-CHOL membrane because dioscin is expected to stay in the outer leaflet of the membrane first, and would take time and energy to penetrate into the membrane.

For each of the CGMD simulations mentioned above, the given system was first minimized until convergence. Then, a 5 ns position-restrained MD simulation for water was performed to optimize the bilayers and to avoid penetration of water into the un-equilibrated bilayer. Finally, 400 ns production simulations were run under NPT ensemble (T = 310 K and P = 1 atm) using the Berendsen thermostat and barostat, and the pressure coupling was applied in a semi-isotropic manner. During simulation, the non-bonding interaction distance cutoff was set at 12 Å. The Lennard-Jones potential was shifted from $R_{shift} = 9$ Å to R_{cutoff}. The electrostatic potential is shifted from $R_{shift} = 0$ Å to R_{cutoff}. The neighbor list was updated every ten steps. The integration time interval was 20 fs. Equilibration of the bilayer was monitored by the average area per lipid molecule. Interpretation of the time scale in CG simulations was not straightforward. The simulation time may need rescaling by a factor of 1/4 to be comparable with the results of all-atom simulation or real time [26]. However, different processes or systems may have different conversion factors. For the sake of convenience, we did not rescale the simulation time in our study since real time scale was not relevant to the purposes of our study.

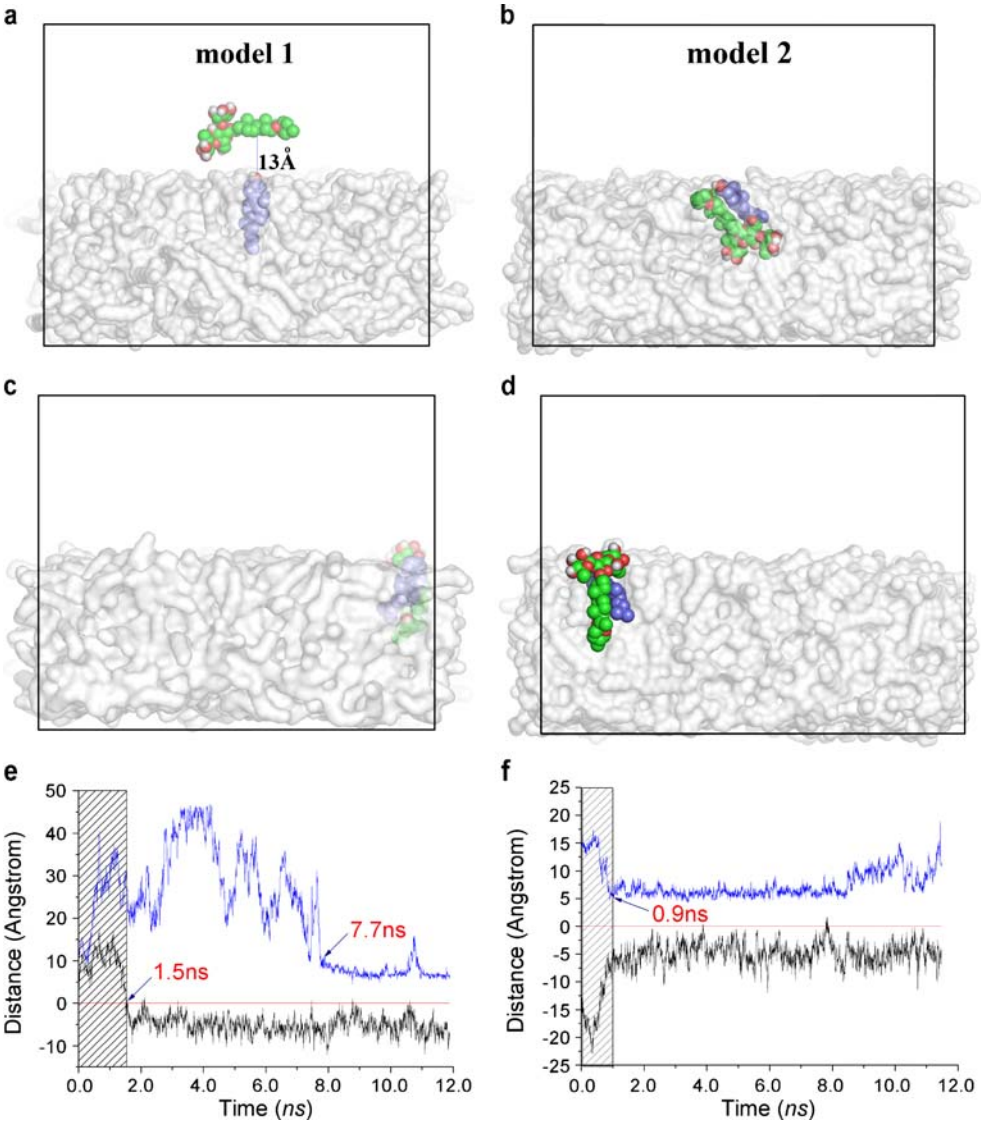

Fig. 4 **a** Initial configuration of MD model 1, in which a dioscin molecule was placed in water above a cholesterol molecule in decane; the distance between them was 13 Å. **b** Initial configuration of MD model 2, with a dioscin molecule bound with a cholesterol molecule in the head-to-tail mode in decane; the decane phase is rendered in *gray* while all water molecules are hidden in this figure. **c** The last snapshot of the MD simulation initiated from model 1. **d** The last snapshot of MD simulation initiated from model 2. **e**, **f** Distance fluctuations during MD simulations initiated from models 1 (**e**) or 2 (**f**). *Red lines* Water–decane interface, *black curves* distances between water—decane interface and a certain oxygen atom on dioscin, *blue curves* distance between a certain oxygen atom on cholesterol and a certain oxygen atom on dioscin

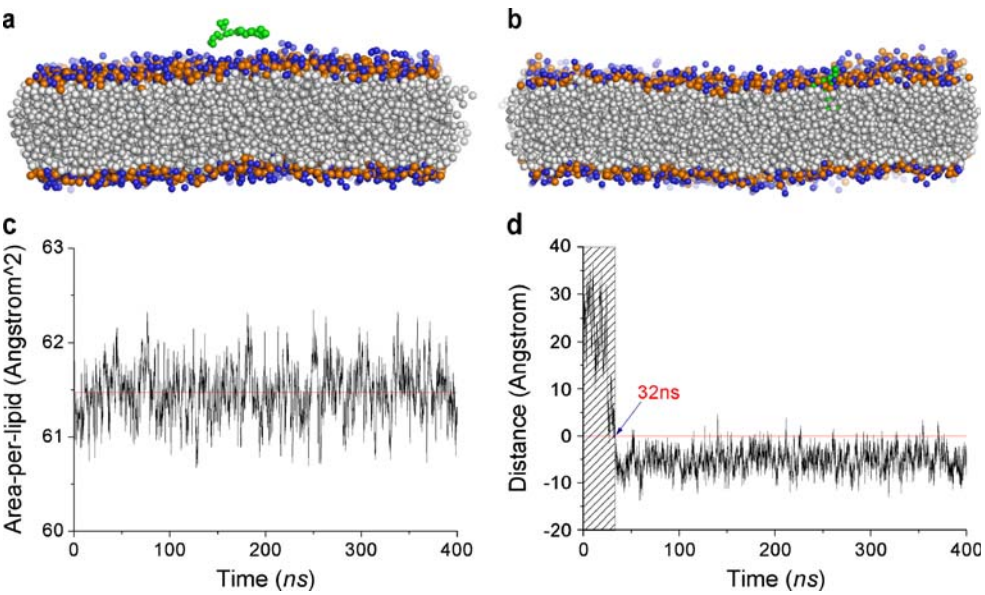

Fig. 5 **a** The initial configuration of dioscin on a DPPC bilayer for coarse-grained molecular dynamics (CGMD) simulation. Dioscin is colored *green*, and placed on top of a bilayer of 1,024 DPPC molecules. Each *sphere* stands for an interaction site used by the CG model. **b** The last snapshot of a 400 ns MD simulation. **c** Fluctuation of area per lipid molecule during the MD simulation. **d** Fluctuation of the distance between dioscin and the bilayer surface during MD simulation. Positive values indicate that dioscin is outside the bilayer, while negative values indicate that dioscin is inside the bilayer

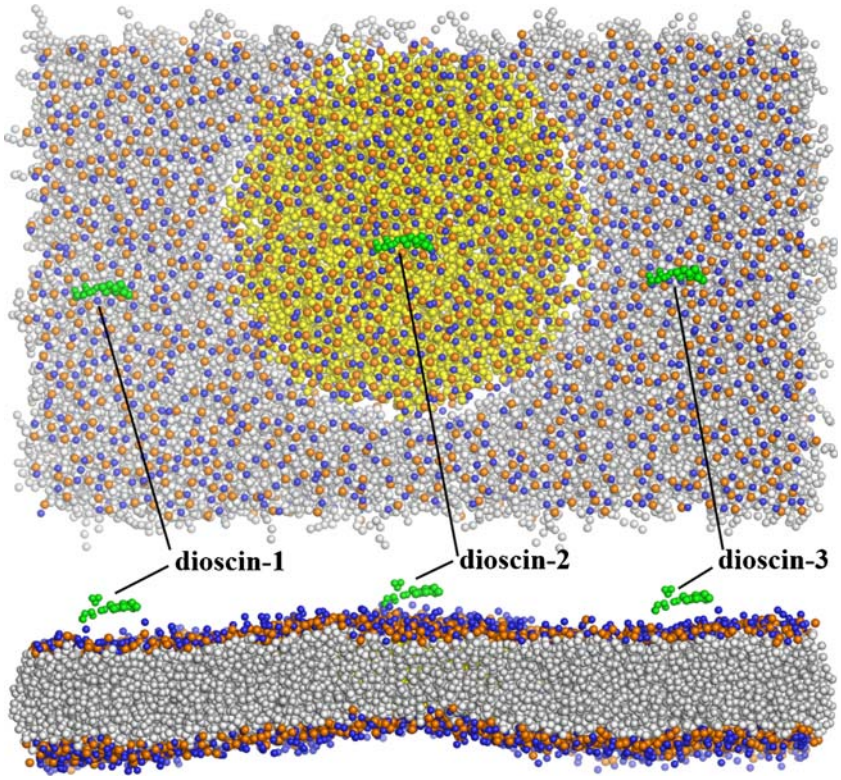

Fig. 6 The initial configuration of the DPPC-POPC-PSM-CHOL system for CGMD (*top* - and *side-view*). The *yellow round area* at the center of the DPPC membrane is the POPC-PSM-CHOL lipid raft micro-domain. Three dioscin molecules are colored in *green*

Results and discussion

Stabilities of the dioscin–cholesterol complex and the cholesterol–cholesterol complex

Our MM-GB/SA computation results (Table 2) indicate that the binding free energy of the dioscin–cholesterol complex in decane is much lower than that of the cholesterol–cholesterol complex (−19.10 kcal mol^{-1} vs −0.77 kcal mol^{-1}). Thus, the stability of the dioscin–cholesterol complex in decane is predicted to be much stronger than that of the cholesterol–cholesterol complex. One reason is that dioscin has a large oligosaccharide moiety, which forms additional electrostatic interactions with cholesterol. As seen in Table 2, the electrostatic interaction energy between dioscin and cholesterol in vacuum (−10.47 kcal mol^{-1}) is much lower than the equivalent interaction between cholesterol and cholesterol (−0.01 kcal mol^{-1}). Another reason comes from the solvation effect. The data in Table 2 show that solvation free energy favors the formation of the dioscin–cholesterol complex in decane much more than in water.

Our results also indicate that the binding free energy of the dioscin–cholesterol complex in water is also lower than that of the corresponding cholesterol–cholesterol complex (−3.38 kcal mol^{-1} vs 0.49 kcal mol^{-1}). Also, one can see that the binding free energy of the dioscin–cholesterol complex in decane is much lower than that in water (−19.10 kcal mol^{-1} vs −3.38 kcal mol^{-1}). This can be explained by the solvation free energy terms in Table 2. The solvation free energy of the dioscin–cholesterol complex into decane is much lower than that of the same complex into water (−12.89 kcal mol^{-1} vs 0.12 kcal mol^{-1}), which indicates that formation of the dioscin–cholesterol complex is favored by the solvation effect in decane over that in water.

Assuming that the ratio between cholesterol in red cells and dioscin in the HD_{50} hemolytic assay is 100:1, the concentration ratio between the dioscin–cholesterol complex and the cholesterol–cholesterol complex in either decane or water can be estimated according to the MM-GB/SA binding free energy and the equilibrium between free dioscin, free cholesterol, and the dioscin–cholesterol complex. Our results show that the ratio between the dioscin–cholesterol complex and the cholesterol–cholesterol complex in decane (15.5:1) is 330 times greater than it is in water (0.05:1). The solvent of decane used in our MD simulations in fact mimics the non-polar environment inside a lipid membrane. Thus, we conclude that the stronger affinity inside the membrane may be the driving force for dioscin to partition into the membrane, where it may form a stable dioscin–cholesterol complex.

These MD simulations provide some clues as to the hemolytic mechanism of dioscin. Glauert [6] pointed out that the production of pits and holes in a lipid membrane by saponin does not result from the removal of cholesterol

Table 2 Binding free energies of the dioscin–cholesterol and cholesterol–cholesterol complexes in water and in decane computed by MM-GB/SA[a]

System	In water				In decane			
	Dioscin–cholesterol		Cholesterol–cholesterol		Dioscin–cholesterol		Cholesterol–cholesterol	
	Mean	SD	Mean	SD	Mean	SD	Mean	SD
ΔELE	−2.19	3.41	−0.04	0.53	−10.47	1.71	−0.01	0.25
ΔVDW	−17.94	3.14	−14.88	1.77	−14.66	3.39	−10.87	3.83
ΔINT	−0.02	0.02	0.00	0.00	2.36	1.84	0.82	1.09
ΔG_{GAS}	−20.15	3.91	−14.92	1.86	−22.77	3.37	−10.06	3.57
ΔGB_{SUR}	−1.13	0.19	−0.95	0.11	−1.14	0.20	−0.70	0.24
ΔGB	1.25	1.23	2.03	0.58	−11.75	3.83	−3.28	1.00
ΔGB_{SOL}[b]	0.12	1.28	1.08	0.56	−12.89	3.98	−3.98	1.20
TΔS	−16.67	1.31	−14.33	0.83	−16.56	1.12	−13.23	1.44
ΔH[c]	−20.05	3.90	−13.84	1.73	−35.66	6.47	−14.04	4.56
ΔG[d]	−3.38	3.53	0.49	1.64	−19.10	5.96	−0.77	3.89

[a] All energies are in kcal mol^{-1}

[b] $\Delta GB_{SOL} = \Delta GB + \Delta GB_{SUR}$

[c] $\Delta H = \Delta G_{GAS} + \Delta GB_{SOL}$

[d] $\Delta G = \Delta H - T\Delta S$ (T=300K)

from the membrane by saponin, but rather penetration of saponin into the membrane. Sarjeet et al. also reported [28] that saponin bound cholesterol and sequestered it from other interactions, but did not extract it from the membrane. According to the free energies computed by MM-GB/SA, the dioscin-cholesterol complex is much more stable inside the membrane. Thus, binding of saponin to cholesterol is more likely to occur inside the membrane, and such an event will not extract cholesterol from the membrane. Our simulations are thus in agreement with experimental observations.

Binding modes of the dioscin–cholesterol complex

Our MD simulations not only predict the energetics of the dioscin-cholesterol binding process, but also provide some details on the possible binding modes between dioscin and cholesterol, which is difficult for other experimental techniques to observe directly. According to the cluster- and RMSD-analysis (Fig. 3, and Figs. S2, S3), we can see that all the binding modes between dioscin and cholesterol are head-to-head mode (which means that the oligosaccharide part of dioscin is closest to the hydroxyl group of cholesterol) in decane and water. The conformation of dioscin and cholesterol complex in water is more diverse than it is in decane, which may be one of the reasons for the above conclusion that the binding ability for dioscin and cholesterol in water is much weaker than it is in decane. In water, the binding mode is much more complicated; Fig. S3 shows seven typical conformations.

There are two main clusters of low-energy conformations of the dioscin–cholesterol complex in decane. An interesting observation on the RMSD curve in the MD simulations (Fig. 3a) is that one turning point exists around 5 ns, which corresponds to a turning point on the MM-GB/SA energy curve (Fig. 3c). On the RMSD curve, this turning point can divide the whole trajectory into two clusters: D-1 and D-2. The MM-GB/SA free energy of D-2 is lower than that of D-1. The difference of binding mode between D-1 and D-2 can be seen from Fig. S2. For the D-1 cluster, the oligosaccharide of dioscin adopts the extended form, and the cholesterol is quite parallel with the steroid part of dioscin. However, for the D-2 cluster, the oligosaccharide of dioscin is folded to form a hydrogen bond with the hydroxyl group of cholesterol, which can explain why the D-2 cluster is favorable in MM-GB/SA free energy in Fig. 3c.

There is one turning point at 1.5 ns on the black curve in Fig. 4e, which means that dioscin penetrates into the decane phase. However, it is still far away from the cholesterol molecule, because the blue curve indicates that the dioscin–cholesterol complex is not formed until 7.7 ns. Then, both curves level off, indicating that the entire system is well equilibrated. The last snapshot of the MD simulation is shown in Fig. 4c, so we can divide the whole process into three parts. Firstly, dioscin in water penetrates into the decane. Secondly, dioscin and cholesterol move in the decane, respectively. Thirdly, the dioscin–cholesterol complex forms spontaneously in decane. This is further informed by the predicted logP value of dioscin (no

experimental logP value of dioscin is available). From the predicted logP value (1.34, 1.16 and 1.54 are given by XLOGP3, AlogP98 and ALOGPS, respectively) [29–31], we can see that the overall effect of dioscin is inclined to the lipophilic environment, even though dioscin has a hydrophilic oligosaccharide moiety.

From this simulation, one can also see that binding between dioscin and cholesterol is primarily in the head-to-head mode. However, one cannot exclude the possibility of the head-to-tail mode, i.e., the oligosaccharide moiety of dioscin close to the side chain of cholesterol, because some cholesterol derivatives are observed to pack in an anti-parallel way in crystal structures [23–25]. Thus, we further examined whether dioscin and cholesterol would form a stable head-to-tail binding mode in the decane/water two-phase system, which mimics the environment of the inner and outer regions of a lipid membrane.

Figure 4f shows that both curves have a turning point in the snapshot at 0.9 ns. The shaded area indicates that the oligosaccharide part of dioscin is not favorable in decane, and rotation of dioscin makes the oligosaccharide part of dioscin extend toward the water phase. After this turning point, both curves level off, and this equilibrated part of the curves is very similar to its counterpart in the above simulation. The last snapshot of the MD simulation is shown in Fig. 4d. So, we can see that the head-to-tail mode of the dioscin–cholesterol complex spontaneously transformed into head-to-head mode, which indicates that the head-to-tail mode is not stable in the decane/water two-phase system, even though it exists in the crystal structure of the cholesterol derivative. So far, we have used only the decane/water two-phase model and limited time scale to model this process, which also indicates that dioscin may first penetrate into red cell membranes and interact with cholesterol (which is rich in lipid rafts) to cause a hemolytic process. Now we turn to CGMD simulations to give us more information about this process.

Possible hemolytic mechanism of dioscin

In this study, we performed lengthy CGMD simulations of the behavior of dioscin molecules on some lipid bilayer models, hoping to explore the possible hemolytic mechanism of dioscin. As described in the Methods section, the first set of such simulations was conducted on a model of a DPPC bilayer. Initially, one dioscin molecule was positioned in the water above the DPPC bilayer and a 400 ns CGMD was performed. From Fig. 5c, we can see that the system is well equilibrated, and the average area of the cross-section of each lipid molecule is 61.500 $Å^2$, which is near the experimental value (64.000 $Å^2$) of area per lipid for DPPC at 328 K. The last snapshot of the MD simulation is shown in Fig. 5b. One can see in Fig. 5d that there is a turning point around 32 ns, indicating that dioscin crosses the membrane–water interface to enter the membrane. We thus conclude that penetration of dioscin into the lipid membrane is relatively easy and fast.

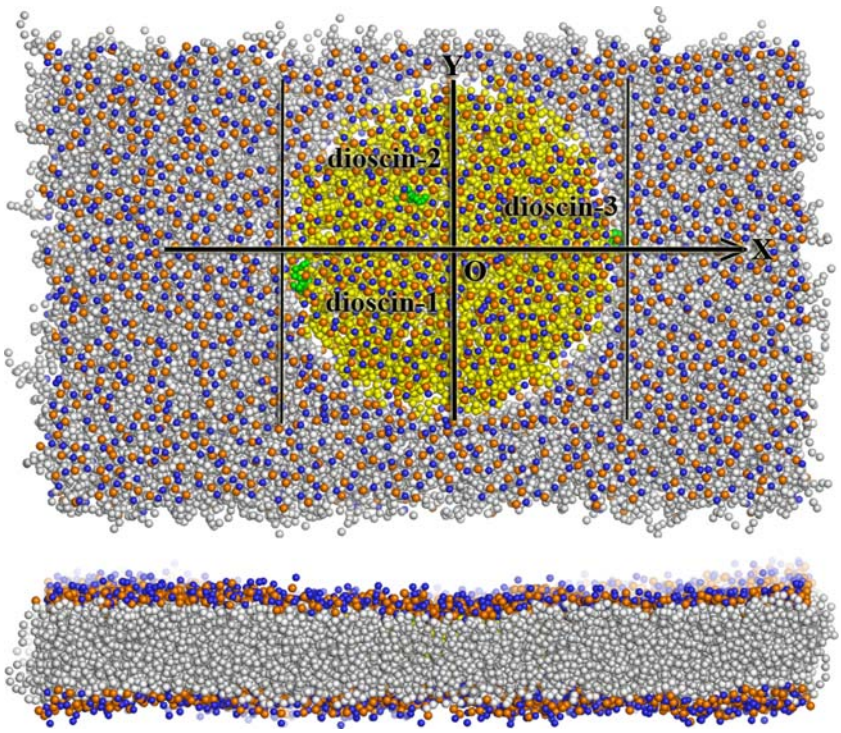

Fig. 7 Top view and side view of the last snapshot after CGMD simulation of three dioscin molecules on the DPPC-POPC-PSM-CHOL membrane

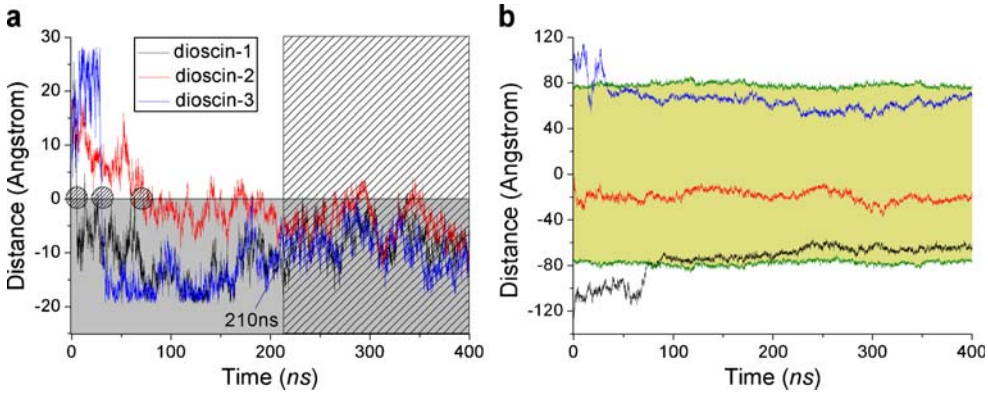

Fig. 8 **a** Distances between three dioscin molecules and the membrane surface during CGMD simulation. Positive values indicate that a given dioscin molecule is outside the membrane; otherwise it is inside the membrane. The three dioscin molecules were placed initially above the membrane before simulation started. **b** Size of the lipid raft micro-domain during CGMD simulation. The *green curves* indicate the lower and upper boundaries of the lipid raft projected onto the X axis. The *black*, *red*, and *blue curves* indicate the positions of three dioscin molecules projected onto the *x*-axis

In order to explore how dioscin interacts with the lipid raft, i.e., the cholesterol-rich micro-domain, we performed CGMD simulations. As shown in Fig. S7, the entire system (DPPC: POPC: PSM: CHOL: DIOSCIN = 1644: 256: 128: 128: 3) is well equilibrated and the average area per lipid molecule is about 53.700 Å^2, which is smaller than DPPC area per lipid at 310 K, while the average area per lipid in the lipid raft micro-domain is about 40.098 Å^2, and this micro-domain is relatively compact compared to other part of lipid (whole membrane excluding micro-domain is shown in Fig. 6; the average area per lipid of this part is 63.466 Å^2). This point is further illustrated in Fig. 8a—the dioscin (dioscin-2) above the micro-domain takes longer than the others (dioscin-1 and dioscin-3) to penetrate into the membrane. One major reason is that the lipid raft micro-domain (Fig. 7) is much more compact than the other part (the whole membrane excluding the lipid raft micro-domain is shown in Fig. 7). It is very interesting that the three curves in Fig. 8a converge after 210 ns in our simulation, which implies that the three dioscin molecules have been accommodated into the lipid raft micro-domain, and that this micro-domain has reached an equilibrium state.

Because this micro-domain is more compact than the other parts of the membrane, its charge density is also relatively higher. Note that dioscin has a large oligosaccharide moiety that is also highly polar. Thus, there is a strong tendency for dioscin to move towards this micro-domain, resulting in accumulation of dioscin in this micro-domain, which can be seen from Figs. 7 and 8b. According to this simulation, we conclude that dioscin first penetrates the membrane much more easily than the other lipid raft micro-domain, and then swims towards this micro-domain spontaneously.

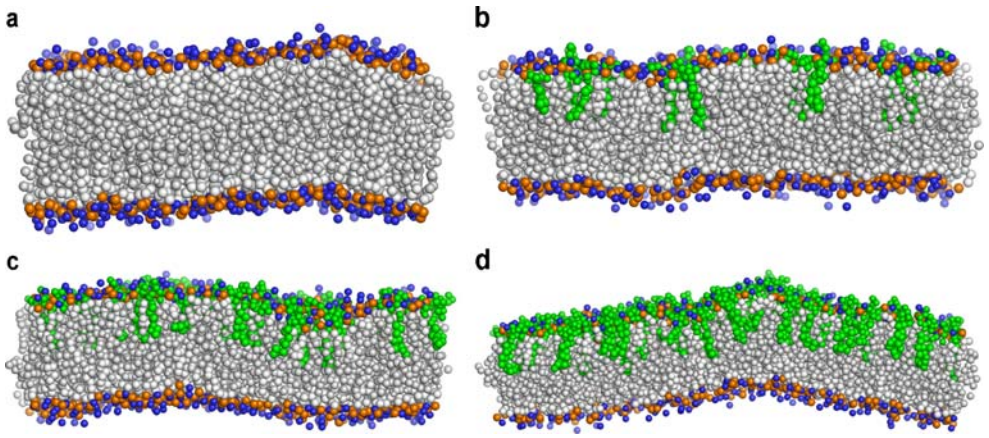

Fig. 9 The last snapshots of four CGMD simulations of the POPC:PSM: CHOL:dioscin system with different compositions: POPC: PSM: CHOL: dioscin = 256:128:128:0 (**a**), 256:128:128:32 (**b**), 256:128:128:64 (**c**), and 256:128:128:128 (**d**). Each *sphere* stands for an interaction site in the coarse-grained model. Dioscin molecules are rendered in *green*, and were initially placed on the upper leaflet of the bilayer. Each CGMD simulation was 400 ns long

As more and more dioscins accumulate in this micro-domain, we still do not know what kinds of effects will be produced. Accordingly, we conducted four sets of CGMD simulations of the POPC-PSM-CHOL-DIOSCIN system with different compositions (POPC: PSM: CHOL: DIOSCIN = 256: 128: 128: 0, 256: 128: 128: 32, 256: 128: 128: 64, and 256: 128: 128: 128) to observe the effect caused by the accumulation of dioscin molecules in the lipid raft micro-domain. One can see in Fig. 9 that, as more and more dioscin molecules accumulate in the lipid raft, membrane curvature becomes more and more obvious. This observation prompts the conclusion that membrane curvature is dioscin dose-dependent, and that the lipid raft micro-domain may be deconstructed once enough dioscin molecules accumulate in this region.

In summary, our CGMD simulations indicate that entering of dioscin molecules into the membrane will cause two effects. Firstly, binding between dioscin and cholesterol, as studied by our all-atom MD simulations, may sequester cholesterol from interactions with sphingomyelin, and this will damage the structure of the lipid raft micro-domain (cholesterol is believed to interact with sphingomyelin in the lipid raft [32]). Secondly, as more and more dioscin molecules accumulate in the lipid raft micro-domain, the morphology of the membrane will be distorted because the dioscin molecule does not have a compact shape like other native molecules in the lipid raft micro-domain. These two factors collectively destabilize the lipid raft, which may eventually lead to membrane deconstruction, and thus the hemolysis of red cells.

Conclusions

In this study, we first derived representative low-energy conformations of dioscin in vacuum through systematic conformation sampling. Then, we determined, through MM-GB/SA computations, that the dioscin–cholesterol complex is energetically more favorable in a non-polar environment (such as decane) than in water, which is consistent with Glauert and Sarjeet's observation that dioscin is likely to penetrate into membranes and to interact with cholesterol in lipid membranes. Our simulation results suggest that the head-to-head binding mode between dioscin and cholesterol is more favorable in water, decane, or two phases. Third, we proposed a possible hemolytic mechanism of dioscin based on extensive CGMD simulations of dioscin on a lipid bilayer model: dioscin first penetrates into the lipid bilayer, moves towards, and accumulates in, the lipid raft micro-domain, and complexes with cholesterol therein. This will destabilize the lipid raft and cause severe curvature of the lipid bilayer, which may eventually lead to the hemolysis of red cells.

Acknowledgments The authors are grateful for the financial support of the Chinese National Natural Science Foundation (Grants No.20772149 & No. 90813006), the Chinese Ministry of Science and Technology (the 863 high-tech project, Grant No. 2006AA02Z337), and the Science and Technology Commission of Shanghai Municipality (Grant No. 074319113). The crystal structure of cholesterol isobutyl carbonate was provided by Prof. Ja P. Young at Sookmyung Women's University. The MARTINI force field was provided by Prof. Siewert J. Marrink at University of Groningen. The authors are also grateful to Prof. Biao Yu and his student Yibing Wang at the Shanghai Institute of Organic Chemistry for their helpful discussions.

References

1. Martin JP, Debbie D (2005) Adv Drug Delivery Rev 57:465–474
2. George F, Zohar K, Harinder PS, Klaus B (2002) Br J Nutr 88:587–605
3. Martin C, Karen P, Laurence VN (2004) Chem Pharm Bull 52:965–971
4. Steurer S, Wurglics M, Likussar W, Burmistrov K, Michelitsch A, Schubert ZM (1999) Pharmazie 54:766–767
5. Masayuki T, Shigetoshi S, Yasuo T (1991) Phytochemistry 30:3943–3944
6. Glauert MA, Dingle JT, Lucy JA (1962) Nature 196:952–955
7. Takechi M, Tanaka Y (1995) Planta Med 61:76–77
8. Yuldasheva LN, Carvalho EB, Catanho JA, Krasilnikov OV (2005) J Med Biol Res 38:1061–1070
9. Toshiyuki A, Shigekazu T, Ushio S, Shoji I, Hazime Sait (1980) Biochemistry 19:1904–1911
10. Li W, Qiu Z, Wang Y, Zhang Y, Li M, Yu J, Zhang L, Zhu Z, Yu B (2007) Carbohydr Res 18:2705–2715
11. Young JP, Jinmi BM, Young SL (2005) Acta Cryst 61:2312–2314
12. The SYBYL software, version 7.2 (2006) Tripos, St Louis, MO
13. Gold Version 3.1 (2006) The Cambridge Crystallographic Data Centre (CCDC), UK
14. Case DA, Pearlman DA, Caldwell JW, Cheatham T, Wang J, Ross WS, Simmerling C, Darden T, Merz KM, Stanton RV, Cheng A, Vincent JJ, Crowley M, Tsui V, Gohlke H, Duan Y, Pitera J, Massova I, Seibel GL, Singh UC, Weiner P, Kollman PA (2002) AMBER 7. University of California, San Francisco
15. Van der Spoel D, Lindahl E, Hess B, Groenhof G, Mark AE, Berendsen HJ (2005) J Comput Chem 26:1701–1718
16. Frisch MJ, Trucks GW, Schlegel HB, Scuseria GE, Robb MA, Cheeseman JR, Zakrzewski VG, Montgomery JA, Stratmann RE, Burant JC, Dapprich S, Millam JM, Daniesl AC, Kudin KN, Strain MC, farkas O, Tomasi J, Barone V, Cossi M, Cammi R, Mennucci B, Pomelli C, Adamo C, Clifford S, Ochterski J, Petersson GA, Ayala PY, Cui Q, Morokuma K, Malick DK, Rabuck AD, Raghavachari K, Foresman JB, Cioslowski J, V Rotiz J, Stefanov BB, Liu G, Liashenko A, Piskora P, Komaromi I, Gomperts R, Martin RL, Fox DJ, Keith T, AlLaham MA, Peng CY, Nanayakkara A, Gonzalez C, Challacombe M, Gill MW, Johnson B, Chen W, Wong MW, Andres JL, Gonzalez C, Gordon MH, Replogle ES, Pople JA Gaussian, Pittsburgh PA (1998)
17. Cieplak P, Cornell WD, Bayly C, Kollman PA (1995) J Comput Chem 16:1357–1377
18. Jorgensen WL, Chandrasekhar J, Madurs J, Impey RW, Klein ML (1983) J Chem Phys 79:926–935
19. Darden T, York D, Pedersen L (1993) J Chem Phys 98:10089–10092

20. Wang J, Wolf RM, Caldwell JW, Kollman PA, Case DA (2004) J Comput Chem 25:1157–1174
21. Jayaram B, Sprous D, Beveridge DL (1998) J Phys Chem B 102:9571–9576
22. Michael F, John K, Charles L (2001) MMTSB Tool Set, MMTSB NIH Research Resource, Scripps Research Institute
23. Mi HK, Young JP (1989) Bull Korean Chem Soc 10:177–185
24. Boo KK, Myung JC, Young JP (1985) Bull Korean Chem Soc 6:333–337
25. Young JP (2004) Bull Korean Chem Soc 25:751–753
26. Marrink SJ, Risselada HJ, Yefimov S, Tieleman DP, Vries AH (2007) J Phys Chem B 111:7812–7824
27. Perttu SN, Samuli O, Marja TH, Mikko K, Ilpo V (2007) PLoS Comput Biol 3:0304–0312
28. Zhuang MB, Oltean DI, Mez IG, Pullikuth AK, Sobero M, Bravo A, Gill SS (2002) J Biol Chem 277:13863–13872
29. Cheng TJ, Zhao Y, Li X, Lin F, Xu Y, Zhang XL, Li Y, Wang RX (2007) J Chem Inf Model 47:2140–2148
30. Ghose AK, Viswanadhan VN, Wendoloski JJ (1998) J Phys Chem A 102:3762–3772
31. Tetko IV, Tanchuk VY (2002) J Chem Inf Comput Sci 42:1136–1145
32. Jacques F, Nicolas G, Radhia M, Nouara Y (2002) Exp Rev Mol Med 27:1–22